Synthetic Metals 213 (2016) 47–56

Contents lists available at ScienceDirect

Synthetic Metals

journal homepage: www.elsevier.com/locate/synmet

New photodiodes based graphene-organic semiconductor hybrid materials

A. Mekki[a], R.O. Ocaya[b], A. Dere[c], Ahmed A. Al-Ghamdi[d], K. Harrabi[a], F. Yakuphanoglu[c,d,*]

[a] Department of Physics, King Fahd University of Petroleum & Minerals Dhahran, 31261 Saudi Arabia
[b] Department of Physics, University of the Free State, South Africa
[c] Department of Physics, Faculty of Science, Firat University, Elazig 23169, Turkey
[d] Department of Physics, Faculty of Science, King Abdulaziz University, Jeddah 21589, Saudi Arabia

ARTICLE INFO

Article history:
Received 7 November 2015
Received in revised form 23 December 2015
Accepted 29 December 2015
Available online xxx

Keywords:
Graphene oxide
Photodiode
Sensor

ABSTRACT

New photodiodes based graphene-organic semiconductor hybrid materials were fabricated for the first time using sol–gel spin coating technique. The current–voltage characteristics of the Au/GO:coumarin/p-Si/Al diodes were investigated under dark and various illumination intensities. The various junction parameters of the diodes were determined using *I–V*,*C–V* and transient characteristics. The transient photocurrent measurements indicate that Au/GO:coumarin/*p*-Si/Al diodes are very sensitive to illumination and the precise responsivity of the diodes is tunable by adjusting GO:coumarin fraction. The capacitance–voltage–frequency (*C–V–f*) measurements indicate that the capacitance of the diodes depends on voltage and frequency. The capacitance decreases with increasing frequency due to a continuous distribution of the interface states. The ability to tune the photosensitivity in the photoconductive mode through graphene oxide:coumarin weight ratio has been shown to lead to a near-constant sensitivity to illumination for a weight ratio of 0.03GO. The obtained results suggest that Au/GO:coumarin/p-Si/Al diodes can be used as a photosensor in optic communications.

1. Introduction

There is much research interest in graphene at present due to its unique electrical and optical properties. Graphene films are among the most favorable candidates for next generation transparent conductive electrodes [1–3]. Such electrodes have been studied widely over the past decade because of their potential applications in flat panel displays, metal/semiconductor diodes and many other electronic devices. In the present work, we have utilized semiconducting nanocomposites of coumarin–graphene oxide to fabricate the photodiodes. Coumarin and its derivatives have attracted considerable wide research interest in pharmaceuticals for their exciting UV–vis photoresponse properties and industry in the form of dye lasers and high-efficiency dye-sensitized solar cells. The molecules exhibit fluorescence in visible light range, large Stokes shifts, high quantum yields and good solubility [4]. Recent studies have focused on the structure vs. optical property of coumarin to better grasp the electronic operational mechanisms that could lead to better rational designs of more efficient coumarin derivatives for optical device applications [5,6]. There have been a number of scaffolding organic compounds that have been used for a variety of reasons, such as low sheet resistance, high optical transparency. The later can be accounted for by fact that the hybrid electrode can overcome the low work-function and high sheet resistance [7,8]. The coumarin molecule consists of a benzene ring fused together with a lactone ring whose double bond extends the conjugated π-system across the molecule. Conjugated coumarins with many of their derivatives, such as anthracene have been shown to possess the planarity required for rigid structure. This makes them suitable for development on flexible substrate. Their wide energy gaps and high fluorescent quantum efficiency makes them potential candidates for use in UV–vis photo-applications [9,10]. The coumarin interlayer is thought to influence the space-charge region of the Schottky junction thereby increasing the barrier height. The electronic properties of coumarin have also been studied and it was found that increased reaction time leads to a lower sheet resistance on the film [11]. The current–voltage (*I–V*) and capacitance–voltage (*C–V*) characteristics of the coumarin–GO/p-Si junctions having various compositions of GO were studied under dark and illumination conditions. It was observed that the photocurrent of the device increases with increase of GO concentration in the

* Corresponding author at: Firat University, Department of Physics, Faculty of Science, Elazig 23169, Turkey. Fax: +90 424 2330062.
E-mail address: fyhanoglu@firat.edu.tr (F. Yakuphanoglu).

http://dx.doi.org/10.1016/j.synthmet.2015.12.026
0379-6779/

composite. The non-illuminated ideality factors of the diodes having 0.005, 0.01, 0.03 and 0.1% of GO in the coumarin–GO composites were obtained to be 3.803, 4.095, 6.838, and 4.893 respectively. The diode having 0.03GO content consistently exhibited the highest photoresponse performance. The obtained results indicate that coumarin–GO composites have high potential in photosensor applications.

2. Experimental details

The graphene oxide (GO) was synthesized by modified Hummers method as described in the literature [12,13]. The coumarin was dissolved in dicholoro benzene. The synthesized GO was dispersed in deionized water (1.5 mg/ml) using stirring for 10 min. and then, it was ultrasonicated for 2 h. The nanocomposites of coumarin and GO were prepared using coumarin and GO solutions having different weight ratios of GO:coumarin (0.005, 0.01, 0.03 and 0.1). The films of GO:coumarin were coated onto surface of p-Si substrate using a spin coater with 7000 rpm for 60 s. Before deposition of the coumarin–GO composite, the native oxide layer of the silicon substrate was etched by HF and then rinsed in deionized water using an ultrasonic bath for 10–15 min. Finally, the silicon wafer was chemically cleaned according to method based on successive baths of methanol and acetone. Top contact of the diodes was prepared by Au metal. For this, Au metal was evaporated by sputtering system in the form of circles giving a diode contact area of $3.14 \times 10^{-2}\,cm^2$. Surface morphology of the films was investigated using a scanning electron microscopy (SEM). The current–voltage (I–V) characteristics of the diodes were performed with KEITHLEY 4200 semiconductor characterization system. Photoresponse measurements were performed using a solar simulator. The intensity of the illumination was measured using a solar power meter (TM-206).

3. Results and discussion

Fig. 1(a–d) shows SEM images of the GO:coumarin films. As seen in Fig. 1(a–d), the surface morphology of the films is changed with GO contents. As seen in Fig. 1a, the composite is formed from the graphene oxide layer and coumarin capped GO layers. The graphene oxide was capped by coumarin organic layer.

Fig. 2(a–d) shows I–V characteristics of the Au/GO:coumarin/p-Si/Al diode under dark and various illumination intensities and GO concentration. The ability to tune the photosensitivity in the photoconductive mode through graphene oxide:coumarin weight ratio has been shown to lead to a near-constant sensitivity to illumination for a weight ratio of 0.03GO. The typical photodiode characteristics in both forward and reverse bias are observed and can be analyzed by thermionic emission theory [14,15]. Accordingly, the current through a rectifying barrier diode as a function of applied bias voltage (V) and temperature (T) can be written

$$I = I_0 \exp\left[\frac{q(V - IR_s)}{nkT}\right] \quad (1)$$

where I_0 is the reverse saturation current given by

$$I_0 = AA^*T^2 \exp\left(-\frac{q\emptyset_b}{kT}\right) \quad (2)$$

where q is the electronic charge, A is device area, A^* is the effective Richardson's constant equal to $32\,A/cm^2\,K^2$ for p-Si and $\emptyset_b$ is the

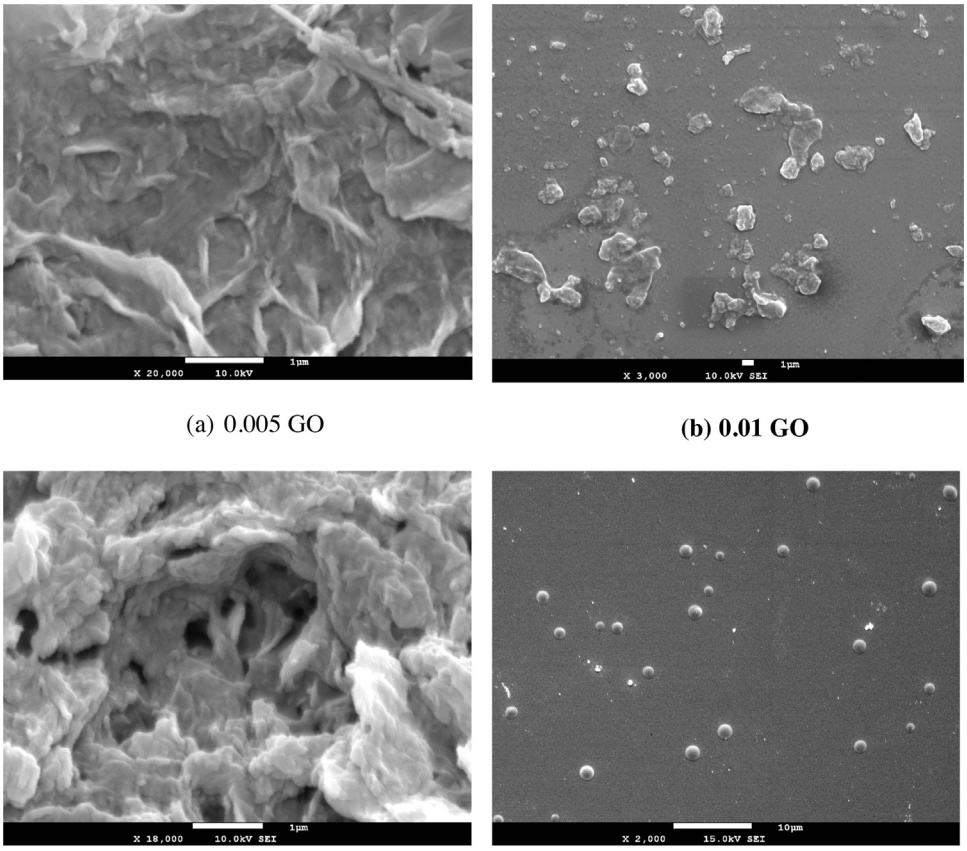

(a) 0.005 GO (b) 0.01 GO

(c) 0.03 GO 0.1 GO

Fig. 1. Scanning electron images at various GO contents taken at the surface of the Schottky diodes.

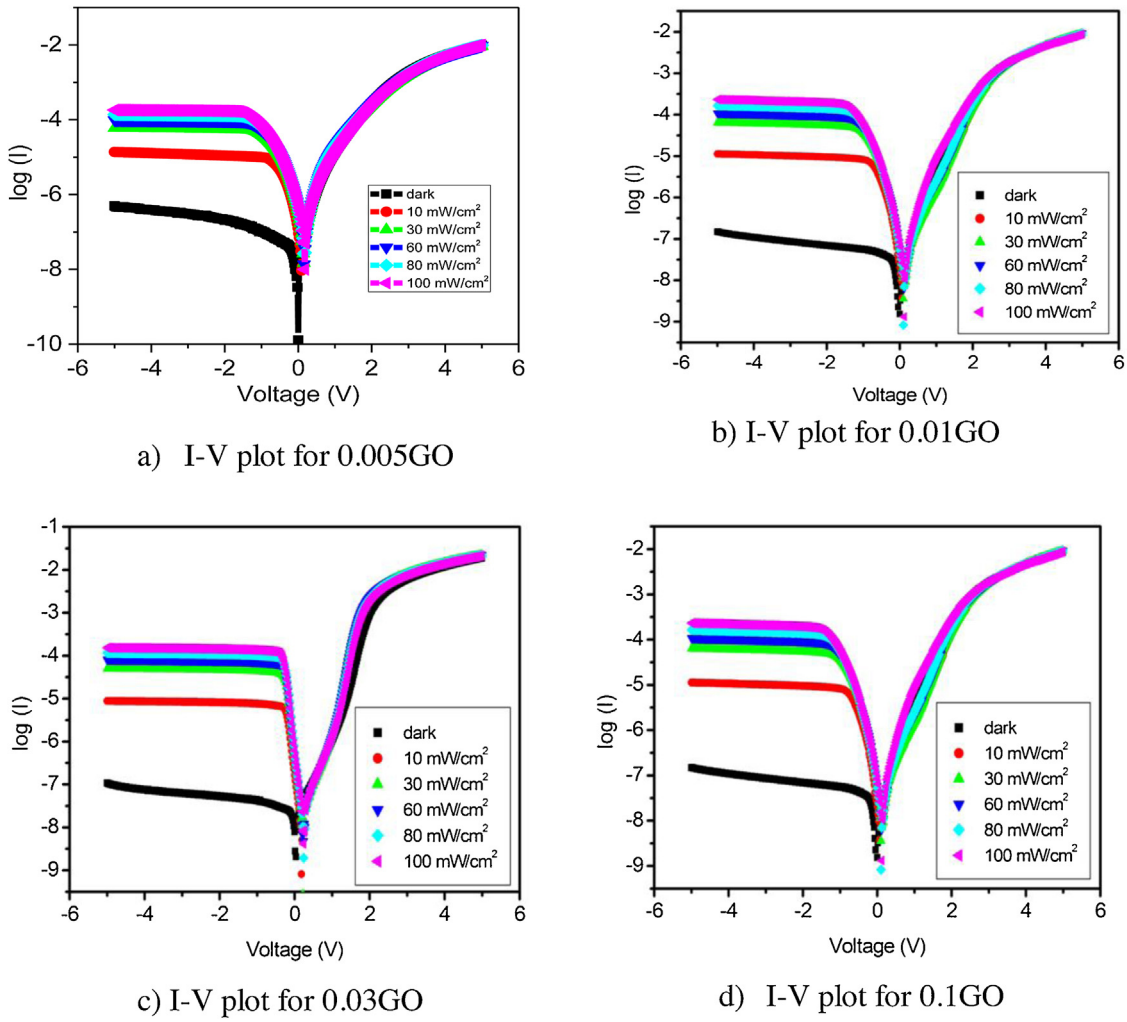

Fig. 2. (a–d) *I–V* characteristics of Au/GO:coumarin/p-Si/Al Schottky diodes at various illumination intensities.

barrier height [16], n is the ideality factor of the diode and k is Boltzmann constant.

Ideality factors greater than unity suggest the presence of barrier height in homogeneities and the existence of interface states. The distribution of interface states can be investigated further through the measurement of the effect of illumination intensity on the diode current. An increase in illumination intensity generates more free carriers with an associated increase in the photocurrent. The photosensitivity of the heterogeneous junction can be investigated through the function

$$I_{PH} = \alpha P^{\gamma} \tag{3}$$

where I_{PH} is the photocurrent, γ is an exponent of the illumination intensity and α is a constant [17,18]. Setting $\alpha = 10^{\beta}$ where β is also constant and taking logarithms of both sides of Eq. (3) gives

$$\log I_{PH} = \gamma \log P + \beta \tag{4}$$

The exponent of the illumination intensity can then be deduced directly from the linear log–log plot of diode current vs. illumination intensity. Fig. 3 shows plots of photocurrent vs. illumination intensity for various GO contents. The calculated exponents at various GO content and reverse bias are given in Table 1.

At the reverse bias voltages of at −3.0 V and −0.2 V the calculated illumination intensity exponents are respectively $\gamma = 1.238 \pm 0.007$ and $\gamma = 0.535 \pm 0.049$. This suggests that a higher magnitude of reverse bias should be used for with similar sensitivity in photo-sensing applications of the diode, regardless of the concentration of GO. However, at 0.03 GO content even lower bias may be used to bias the photodiode. This is potentially attractive for electronic sensing applications that are operated on low supply voltages, such as battery powered photosensors. Values of γ between 0.5 and 1 are believed to indicate the existence of a continuous distribution of localized states in the mobility gap of these materials [18,19]. A higher value of γ obtained for the p-Si/GO–coumarin interlayer indicates a lower density of the unoccupied trap level and suggests a less degraded crystal structure [17,20–22].

A linear dependence of photoconductivity on intensity ($\gamma = 1.0$) suggests that the recombination mechanism is mononuclear, while a square root ($\gamma = 0.5$) suggests a bimolecular recombination mechanism [18]. Fig. 4 therefore suggests that the onset of either one of these mechanisms may be induced through GO:coumarin weight fraction.

Fig. 5 shows semilog plots of dark *I–V* characteristics vs. GO concentrations. The concentration of 0.03 GO shows the lowest magnitude of the reverse current at low applied reverse bias, and

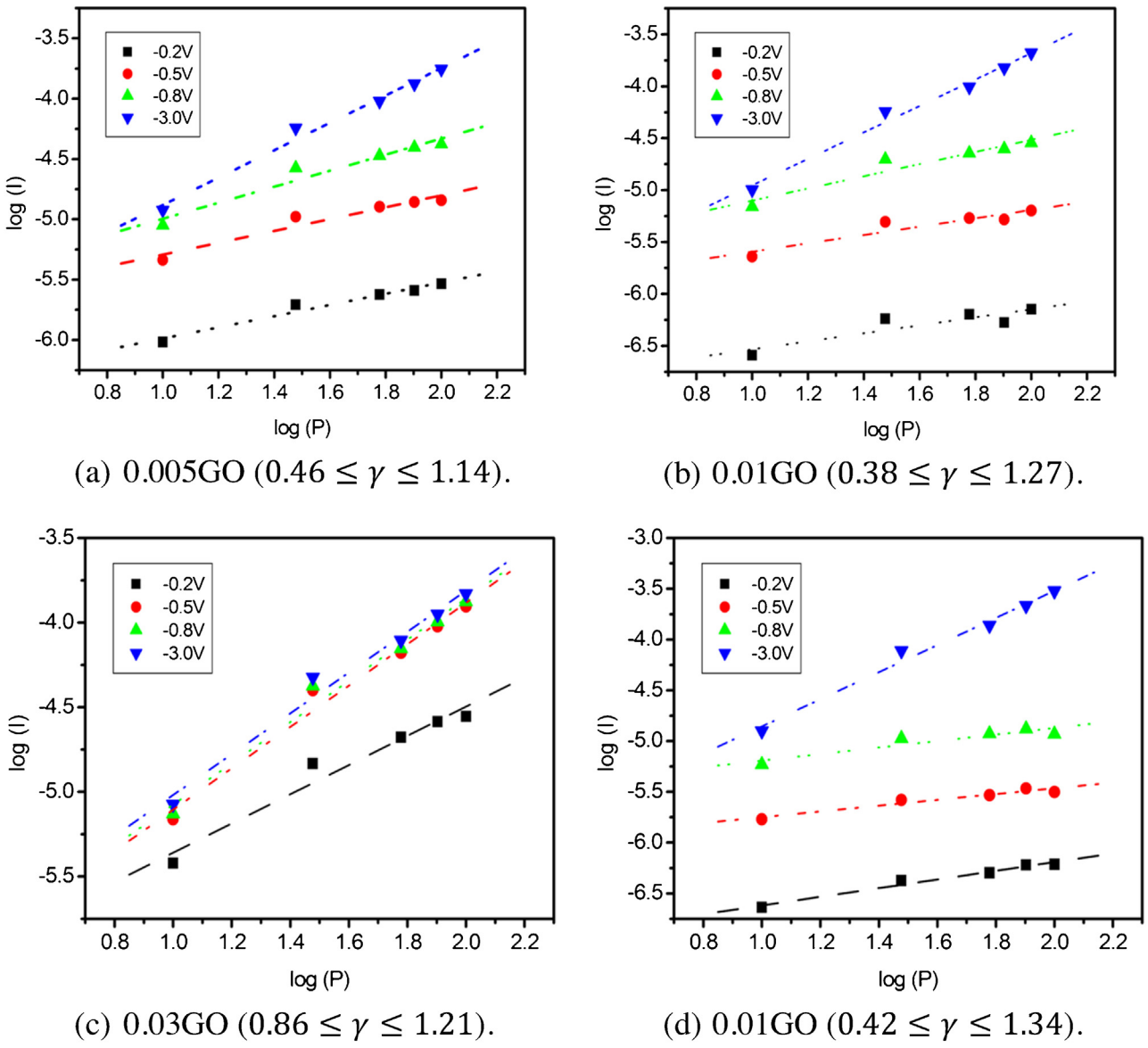

Fig. 3. Plots of photocurrent vs. illumination intensity for various GO contents. These plots show the tunability of the parameter γ in the power law relating diode current with illumination intensity.

there is no discernible correlation between the reverse bias and GO concentration. However, at higher reverse bias the magnitude of the reverse current generally increases with concentration. In the forward bias region, the magnitude of diode current at constant bias generally decreases with GO concentration for concentrations below 0.01GO content. Above 0.01 GO content the forward characteristics exhibit multiple linear regions, which could explain the observed variation in the calculated ideality factor and series resistance. It is not possible with the available data to plot dark current vs. bias voltage in a log–log plot of current vs. intensity.

The deviation from the ideal behavior of the diode can be postulated on the basis of series resistance, which can be determined using Cheung method [23]. In this method, the gradient of the plot of $dV/d(\ln I)$ vs. I is series resistance and the intercept is the thermal voltage scaled by the ideality factor i.e.

$$\frac{dV}{d\ln I} = R_s I + n\left(\frac{kT}{q}\right) \tag{5}$$

In the method, a plot of $H(I)$ vs. I is found to be linear over a wide range of currents, i.e.

$$H(I) = R_s I + n\emptyset_b \tag{6}$$

where

$$H(I) = V - n\left(\frac{kT}{q}\right)\ln\left(\frac{I}{AA^*T^2}\right) \tag{7}$$

Table 1
Calculated illumination intensity exponents at various GO contents.

V_{bias} (V)	γ			
	0.005 GO	0.01 GO	0.03 GO	0.1 GO
−0.2	0.464	0.385	0.863	0.427
−0.5	0.492	0.402	1.224	0.285
−0.8	0.664	0.586	1.217	0.322
−3.0	1.136	1.274	1.207	1.335

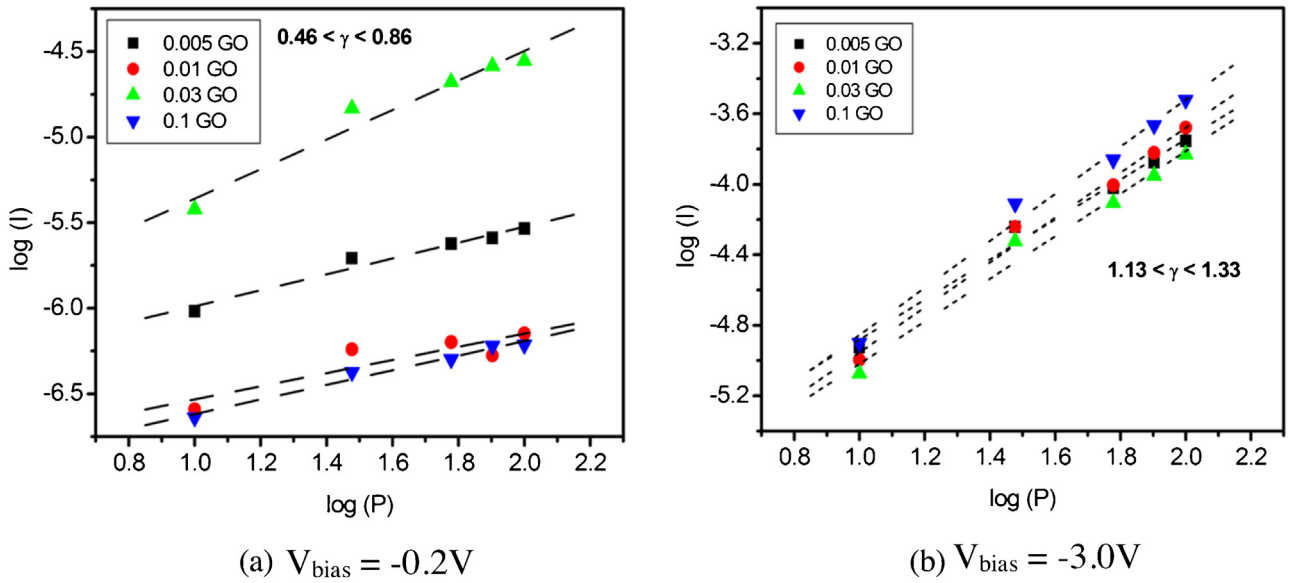

Fig. 4. Variation of the illumination intensity exponent γ with reverse bias voltage.

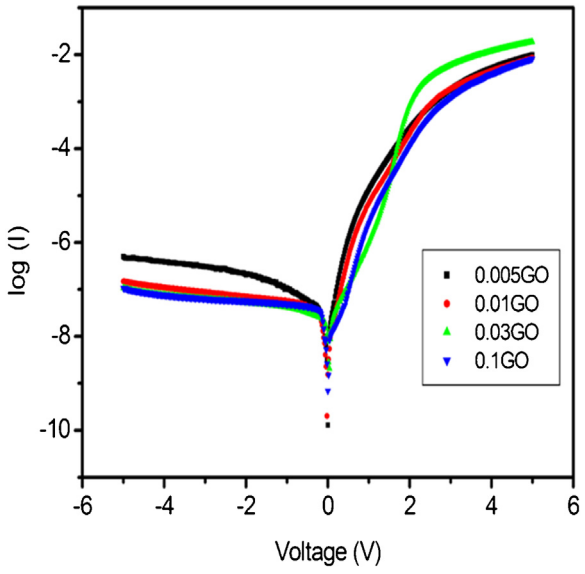

Fig. 5. Semilog plot of dark diode *I–V* characteristics vs. GO concentrations.

Eq. (6) also has a gradient that is equal to the resistance and an intercept that can be used to calculate the barrier potential using the ideality factor from Eq. (5). Fig. 6 shows plots of d*V*/dln*I* and *H* (*I*) vs. current for the Au/GO:coumarin/p-Si/Al diodes with various GO contents and illumination. The obtained ideality factor and barrier height values of the diodes are shown in Table 2.The resistance values obtained using Eqs. (5) and (6) often differ, but the general order of magnitudes are comparable. The differences could be the result of interface states, and the voltage drop across the interfacial layer [24]. Fig. 7 shows plots of barrier height as a function of illumination intensity for various concentrations of GO. As seen in Fig. 7, the barrier height values are changed with GO contents. The highest calculated variation of barrier height at different illumination intensities occured at 0.01 GO concentration. The plots of the variation of series resistance with illumination intensity for the diodes are shown in Fig. 8. The series resistance is changed with GO content and it is decreased with the illuminaton. The obtained series resistance is higher for the diodes. These higher values cause the non-linearity in *I–V* characteristics of the diodes.

Capacitance–voltage and conductance–voltage measurements at various frequencies are popular methods to characterize a Schottky diode. These methods are useful also because the effect of series resistance can be ascertained through the concept of the adjusted capacitance and conductance respectively. From these measurements the barrier height, built-in potential and the density of non-compensated ionized acceptors can additionally be estimated. The capacitance of a junction diode consists of two aspects, namely the diffusion capacitance and the capacitance of the depletion layer across the junction itself. The plots of capacitance–voltage under various frequencies of the diodes are shown in Fig. 9(a–d). As seen in Fig. 9(a–d), the capacitance is changed with frequency. The diffusion capacitance (C_{diff}) is found to vary linearly with illumination intensity and correlates directly

Table 2
Calculated ideality factors and barrier heights vs. GO content at various illumination intensities using Cheung method.

	0		10		30 (mW/cm^2)		60		80		100	
	n	*Φ* (eV)	*n*	*Φ* (eV)	*n*	*Φ* (eV)	*n*	*Φ* (eV)	*n*	*Φ* (eV)	*n*	*Φ* (eV)
GO concentration												
0.005	3.803	0.761	3.569	0.764	3.623	0.761	3.908	0.753	4.067	0.748	5.906	0.721
0.010	4.095	0.792	1.130	0.962	1.029	0.981	1.107	0.960	1.251	0.932	2.708	0.819
0.030	6.838	0.762	1.021	0.996	1.527	0.944	1.621	0.935	4.013	0.817	4.247	0.813
0.100	4.893	0.819	4.071	0.849	4.332	0.835	4.500	0.827	4.780	0.815	5.314	0.801

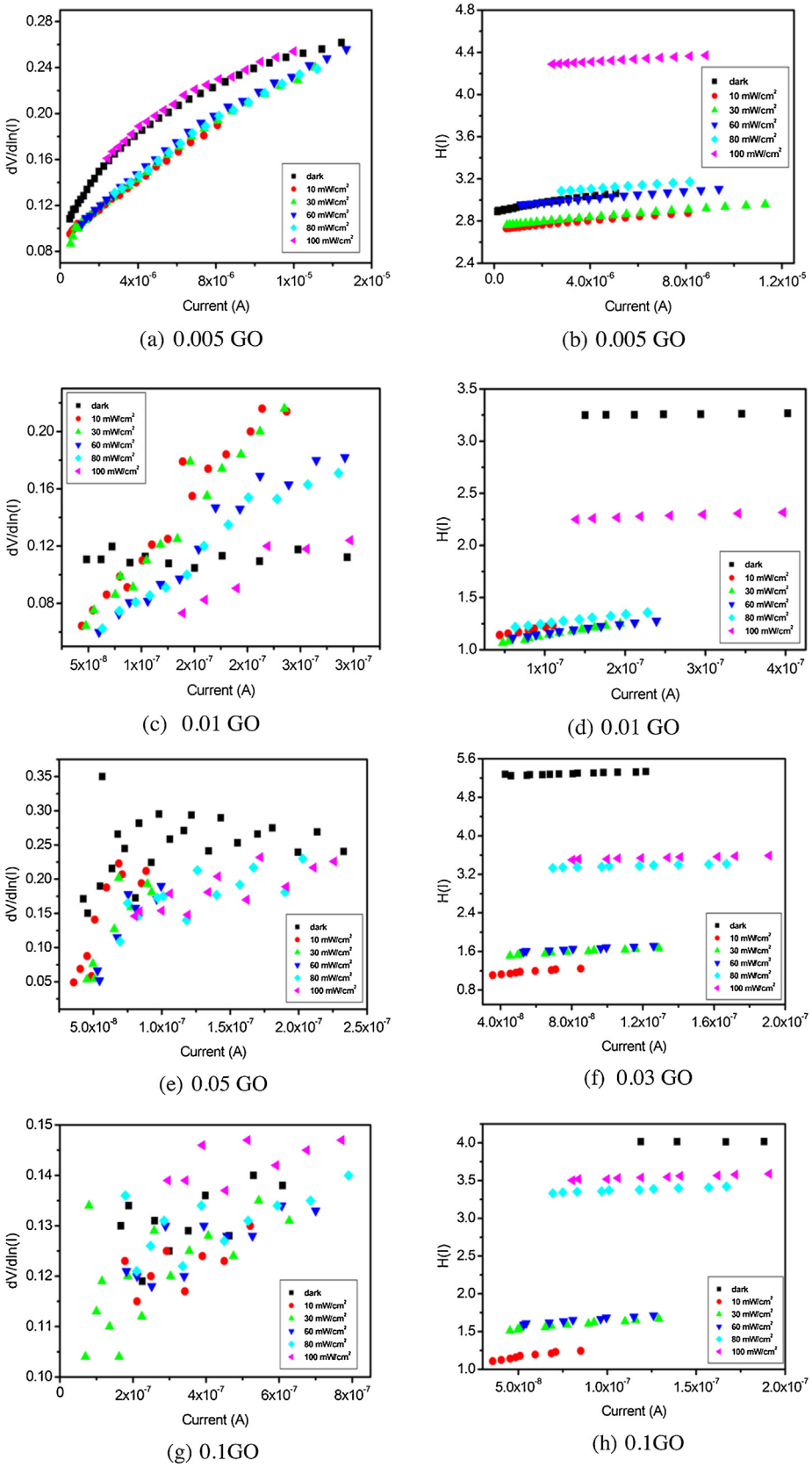

Fig. 6. Plots of d*V*/dln*I* and *H*(*I*) vs. current for the Au/GO:coumarin/p-Si/Al diodes with varied GO content and illumination.

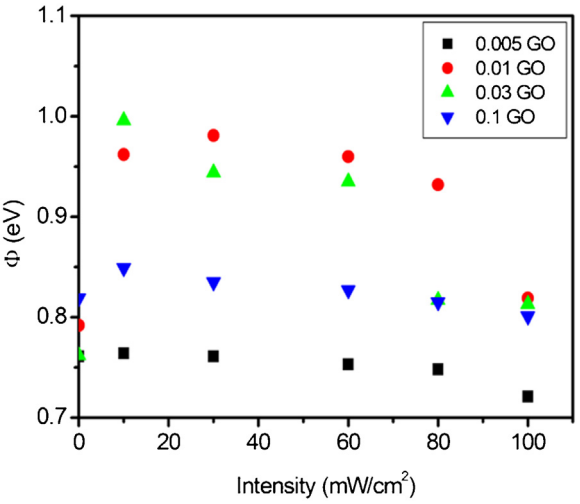

Fig. 7. Plot of barrier height as a function of illumination at various contents of GO.

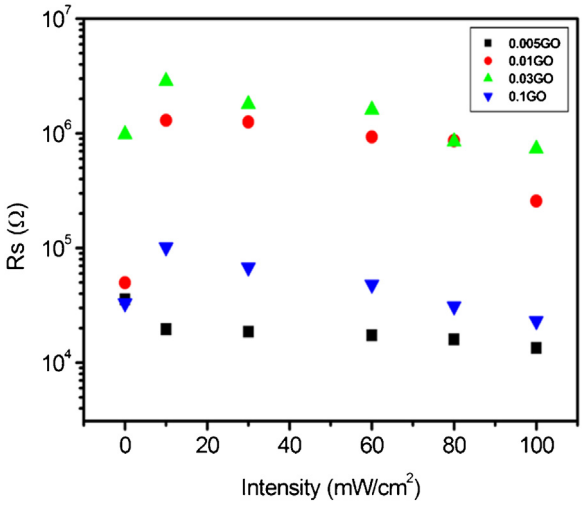

Fig. 8. Semi-log plot of the variation of series resistance with illumination intensity.

with the minority lifetime and is given by [17,25–27]

$$C_{\text{diff}} = \frac{q^2 n_i^2 L_n}{kTN_A}\exp\left(\frac{q}{kT}cV\right) \tag{8}$$

where c is a constant, L_n is the excess minority carrier diffusion length. The depletion layer capacitance (C_{depl}) can be expressed by the following relation,

$$\frac{1}{C_{\text{depl}}^2} = \frac{2}{q\varepsilon_r A^2 N_i}(V_{\text{bi}} + V_r - V_{\text{th}}) \tag{9}$$

where ε_r (11.8 for p-Si) is the dielectric constant, A is the diode area, N_i is the non-compensated ionized acceptor density, V_{bi} is the built-in voltage, V_r is the applied reverse voltage and V_{th} is the thermal voltage equal to (kT/q). At lower temperatures, the thermal voltage contribution is small (typically 0.026 V at room temperature). Fig. 10(a–d) show the plots of C^{-2} vs. V under various frequencies. The plot of (C_{depl}^{-2}) vs. V_r at a given temperature yields ideally a straight line in the reverse bias part of the characteristics from whose gradient N_i can be estimated. Similarly from the ratio of the intercept to the gradient V_{bi} can be estimated [26,28]. The barrier height ($\emptyset_b^c$) from capacitance measurements can be deduced from [29]

$$\emptyset_b^c = V_{bi} + \frac{kT}{q}\left[1 + \ln\frac{N_V}{N_i}\right] \tag{10}$$

where $N_V \approx 1.04 \times 10^{19}\ \text{cm}^{-3}$ is the valence band density of states for the p-Si at 300 K. Eq. (10) is often expressed as [26]

$$\emptyset_b^c = V_{\text{bi}} + V_{\text{th}} + V_P \tag{11}$$

where

$$V_P = \frac{kT}{q}\ln\frac{N_V}{N_i} \tag{12}$$

The effect of illumination on capacitance can be explained in terms of the tunability of the diffusion capacitance, which can be expressed in terms of the photocurrent (I) by

$$C_{\text{diff}} = \frac{\tau}{V_T}I \tag{13}$$

where τ is the minority carrier lifetime [17,27]. The barrier heights based on capacitance measurements are often in disagreement with those measured using other methods, such as $I-V$ and $H(I)-I$, though much effort is currently being expended on addressing the discrepancies which arise from the effects of series resistance and the true-space charge capacitance in the device. A popular method obtains the adjusted capacitance (C_{ADJ}) and conductance (G_{ADJ}) in the light of series resistance and actual space-charge. The two method rely on frequency sensitivities of the junction capacitance and the effective series resistance can be estimated from the real part of the impedance. The corrected capacitance and conductance are expressed respectively [20,30–32] as

$$C_{\text{ADJ}} = \frac{\left[G_m^2 + (\omega C_m)^2\right]}{a^2 + (\omega C_m)^2}C_m \tag{14}$$

$$G_{\text{ADJ}} = \frac{\left[G_m^2 + (\omega C_m)^2\right]}{a^2 + (\omega C_m)^2}a \tag{15}$$

where $a = G_m - \left[G_m^2 + (\omega C_m)^2\right]R_s$.

Table 3 shows the calculated values of non-ionized acceptor concentration, built-in potential, barrier height and potential difference (V_P) between the Fermi level and the bottom of the valence band in the neutral region of the p-Si. The variance in the calculated N_i over the frequency range is less than 1% and the variance in V_P is less than 3 parts per million. However, the barrier height calculated using the C–V is seen to be higher than that calculated using the Cheung–Cheung method. Both the calculated barrier height and the built-in potential are seen to increase with an increase in frequency. The value of N_V, the density of states in the valence band used to calculate the results in Table 3 is $1.04 \times 10^{19}\ \text{cm}^{-3}$ at the characterization temperature of 300 K.

Fig. 11 shows the variation of the series resistance of the Au/GO: coumarin/p-Si/Al Schottky diode with applied bias. The plots exhibit peaks that shift towards the lower positive bias voltage with decreasing frequency, suggesting that the interface states depend strongly on frequency. The high value of series resistance at low frequencies can be explained on the basis that the interface states can follow the AC signal thereby exhibiting excess capacitance at low frequencies [33,34].

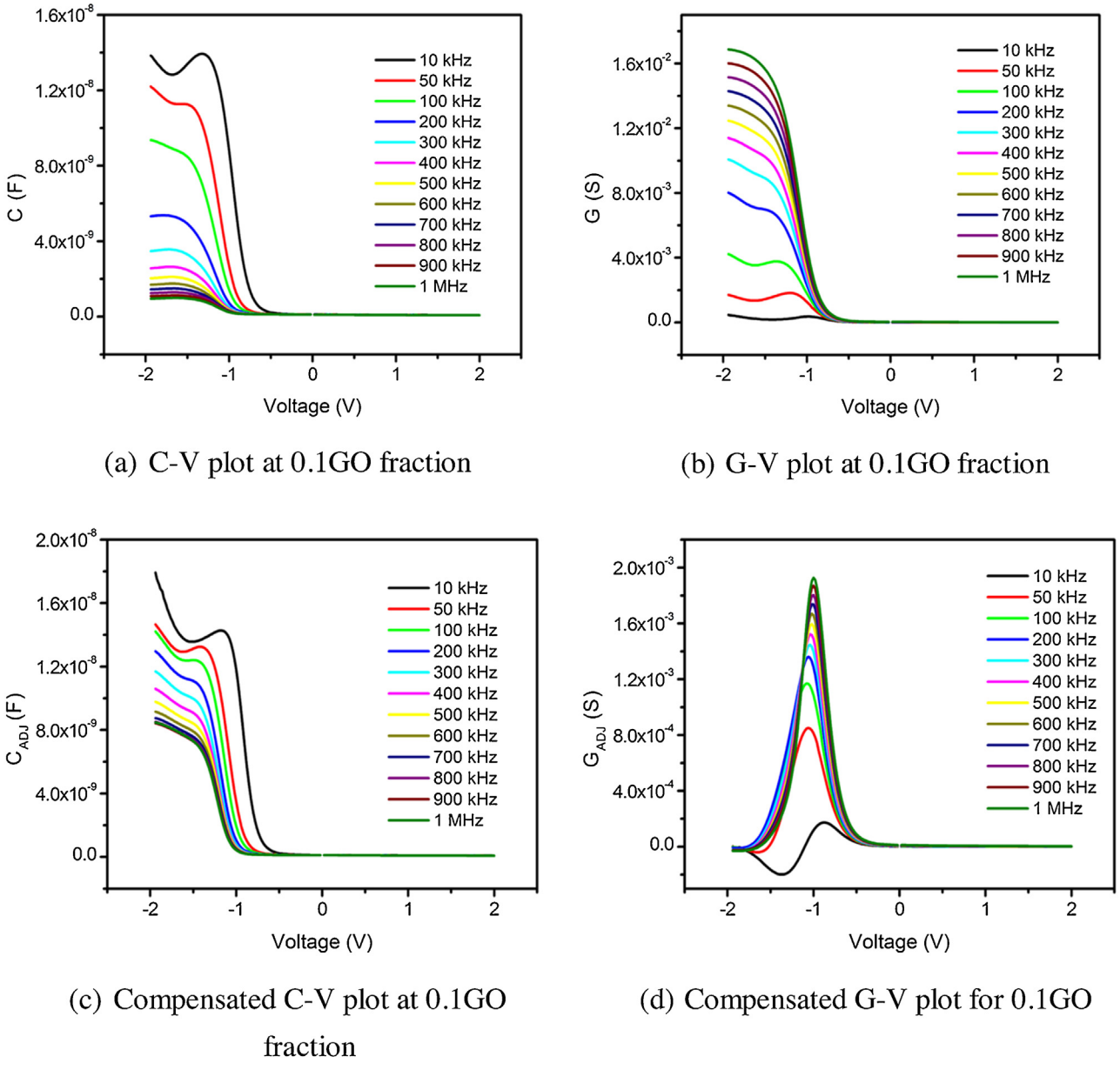

Fig. 9. Frequency dependent capacitance-voltage plots of the diode at 0.1GO content showing the capacitance and conductance respectively, in (a) and (c) uncorrected and in (b) and (d) adjusted.

Fig. 12 shows the transient photocapacitance and photoconductance response of the Al/p-Si/GO:coumarin/Au diode in the forward bias region. The discrepancy between the quasi-steady state and transient measurements in Schottky diodes can be explained in terms of the capacitive current (I_C) which, depending on the measurement conditions, must be combined either additively or subtractively from the photo-generated current. For increasing illumination intensity, i.e., the light is turned on, the diode capacitance is charged and effectively results in a smaller diode current under quasi-steady state. For decreasing illumination, i.e., the light is turned off, the diode capacitance is discharged and the current is larger under quasi-steady state measurement. It follows that [27]

$$I_C = C\frac{dV}{dt} + V\frac{dC}{dt} \tag{16}$$

In forward bias C_{diff} may be neglected, and at quasi-steady state ($dV/dt = 0$) Eq. (14) leads to

$$I_C(t) = -C_0 R_s \exp\left[b\frac{q}{kT}(V - IR_S)\right]\left(1 + b\frac{q}{kT}(V - IR_S)\right)\frac{dI}{dt} \tag{17}$$

from which the diffusion charge (Q_{diff}) can be calculated, using $I_C = \frac{dQ_{diff}}{dt}$. Fig. 13 shows that the photocapacitance and photoconductance depend strongly on GO content.

Fig. 13 shows the photocapacitance and photoconductance depend strongly on the illumination. The initial rise in the capacitance and conductance suggests that more free carriers are generated initially at the junction upon illumination. When the illumination is turned off the capacitance and conductance decay to their initial values, suggesting that trapping of charge carriers occurs in the deep impurity levels. The transient responses suggest

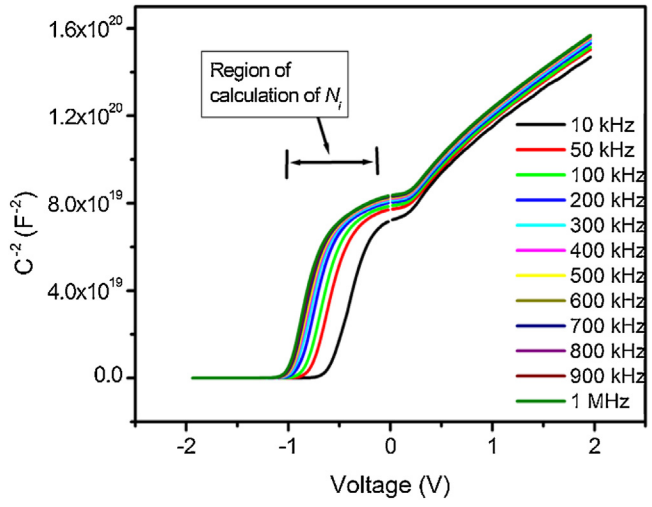

Fig. 10. The reverse bias region of the characteristics illustrated for 0.1GO fraction showing the region at over which the barrier height, density of non-compensated ionized acceptors and the built-in potential were calculated.

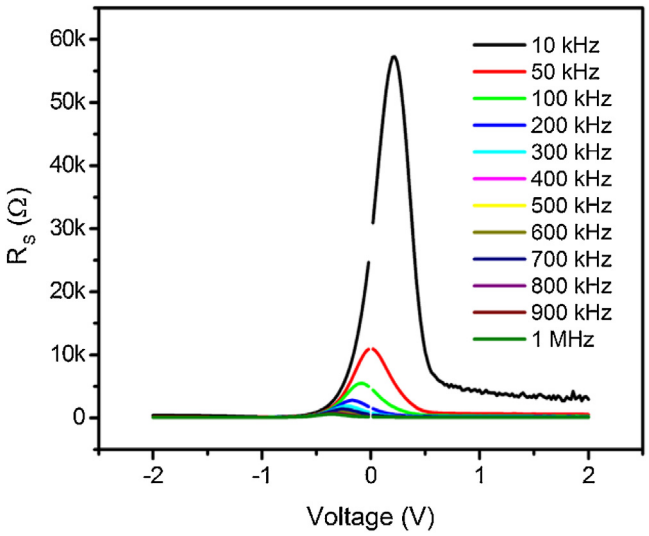

Fig. 11. The voltage dependence of resistance of the Au/GO:coumarin/p-Si/Al diode at room temperature.

Table 3
Electrical parameters calculated using *C–V* measurements at 0.1GO fraction. The non-ionized acceptor concentration averages $(7.287 \pm 0.007) \times 10^{13}$ cm^{-3}).

Frequency (kHz)	N_i (x 10^{13} cm^{-3})	V_{bi} (V)	V_P (V)	$\emptyset_b^c$ (eV)
10	8.36	0.633	0.341	0.974
50	6.93	0.862	0.346	1.208
100	7.26	0.865	0.345	1.210
200	7.18	0.928	0.345	1.273
300	7.31	0.967	0.345	1.311
400	7.17	0.985	0.345	1.330
500	7.37	0.961	0.344	1.305
600	7.36	1.013	0.344	1.358
700	7.37	1.021	0.344	1.365
800	7.40	1.028	0.344	1.372
900	7.44	1.034	0.344	1.378
1000	6.31	1.015	0.348	1.363

that the Au/GO:coumarin/p-Si/Al Schottky diode has potential as a photosensor.

4. Conclusions

Organic on inorganic p-Si Schottky diodes with the structure Au/GO:coumarin/p-Si/Al have been fabricated for the first time. The device parameters were evaluated using current-voltage, capacitance–voltage and phototransient methods with respect to the fraction of graphene-oxide to coumarin ratio. These measurements indicate that the Schottky diode is sensitive to light and there exists the possibility to optimize its performance based on the content of GO. The tunability of the device sensitivity in the photoconductive mode has through adjusting mainly the GO content has been indicated. The best photoresponse was observed for a weight ratio of 0.03 GO.

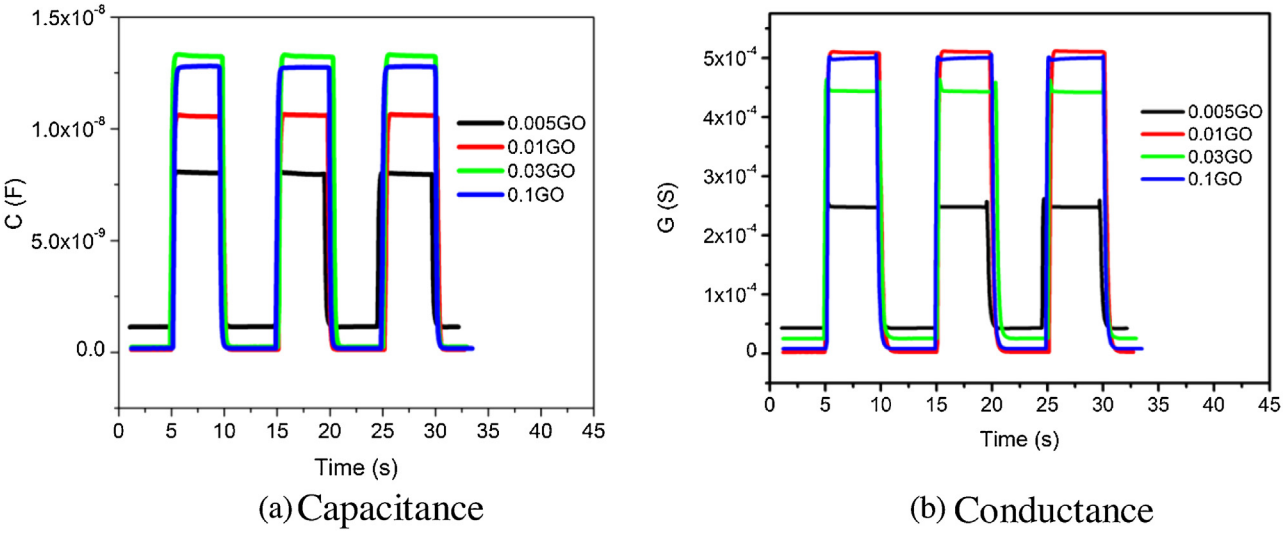

Fig. 12. Transient (forward bias) photocapacitance and photoconductance measurements for Au/GO:coumarin/p-Si/Al diodes.

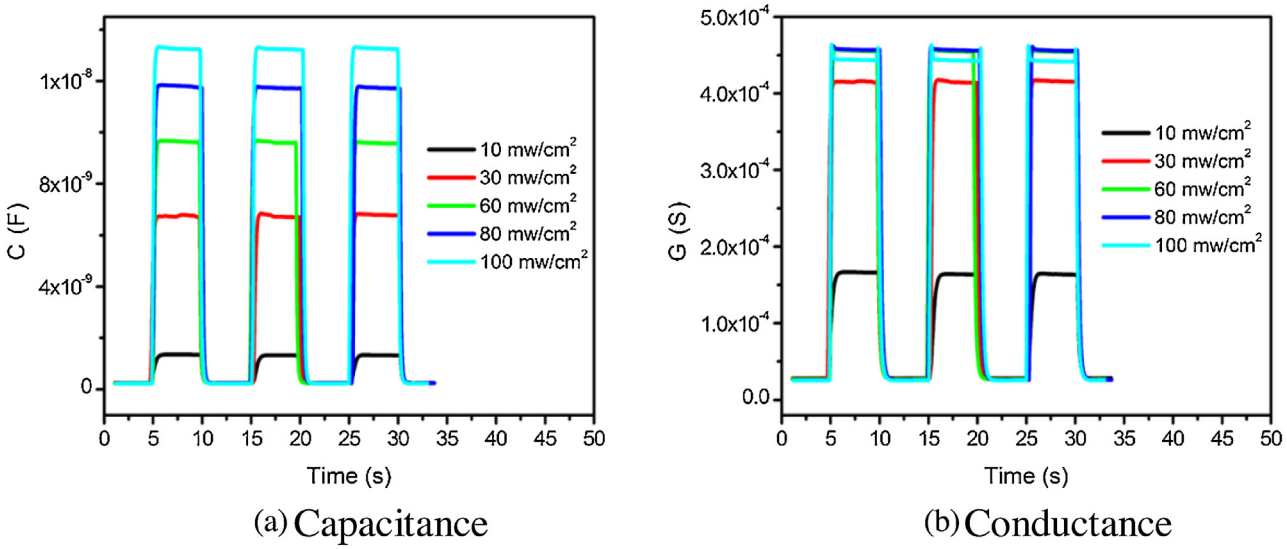

Fig. 13. Transient (forward bias) photocapacitance and photoconductance measurement for the Au/GO:coumarin/p-Si/Al diode at different illumination intensities.

Acknowledgment

Three of the authors (AM, KH & FY) would like to thank The Deanship of Scientific Research at KFUPM for supporting this work under project #IN141009.

References

[1] Y.-Y. Choi, S.J. Kang, H.-K. Kim, W.M. Choi, S.-I. Na, Sol. Energy Mater. Sol. Cells (2012) 281–285.
[2] T. Kuilla, S. Bhadra, D. Yao, N.H. Kim, S. Bose, J.H. Lee, Prog. Polym. Sci. 35 (2010) 1350–1375.
[3] R. Cruz, D.A. Pacheco Tanaka, A. Mendes, Sol. Energy 86 (2012) 716–724.
[4] F.A. Mir, S.U. Rehman, K. Asokan, S.H. Khan, G.M. Bhat, J. Mater. Sci.: Mater. Electron. 25 (2014) 1258–1263, doi:http://dx.doi.org/10.1007/s10854-014-1718-4.
[5] X. Liu, J.M. Cole, P.G. Waddell, T.-C. Lin, J. Radia, A. Zeidler, J. Phys. Chem. A 116 (2012) 727–737, doi:http://dx.doi.org/10.1021/jp209925y.
[6] Z.-S. Wang, K. Hara, Y. Dan-oh, C. | Kasada, A. Shinpo, S. Suga, H. Arakawa, H. Sugihara, J. Phys. Chem. B 109 (2005) 3907–3914.
[7] O.A. Al-Hartomy, R.K. Gupta, A.A. Al-Ghamdi, F. Yakuphanoglu, Synth. Met. 195 (2014) 217–221.
[8] S. Shin, J. Kim, Y.-H. Kim, S.-I. Kim, Curr. Appl. Phys. 13 (Suppl. 2) (2013) S144–S147.
[9] P.-H. Huang, J. -Yi Shen, S.-C. Pu, Y.-S. Wen, J.T. Lin, P.-T. Chou, M.-C.P. Yeh, J. Mater. Chem. 16 (2006) 850–857.
[10] S.S. Razi, P. Srivastava, R. Ali, R.C. Gupta, S.K. Dwivedi, A. Misra, Sens. Actuators B 209 (2015) 162–171.
[11] Y. Chen, K.S. Kang, K.J. Han, K.H. Yoo, J. Kim, Synth. Met. 159 (2009) 1701–1704.
[12] D.T. Phan, R.K. Gupta, G.S. Chung, A.A. Al-Ghamdi, O.A. Al-Hartomy, F. El-Tantawy, F. Yakuphanoglu, Sol. Energy 86 (2012) 2961–2966.
[13] W.S. Hummers, R.E. Offeman, J. Am. Chem. Soc. 80 (1958) 1339.
[14] S.M. Sze, Physics of Semiconductor Device, Second ed., John Wiley & Sons, New York, 1981.
[15] E.H. Rhoderick, R.H. Williams, Metal–Semiconductor Contacts, Second ed., Clarendon Press, Oxford, 1988.
[16] R.K. Gupta, R.A. Singh, Mater. Chem. Phys. 86 (2004) 279–283.
[17] M. Soylu, M. Cavas, A.A. Al-Ghamdi, Z.H. Gafer, F. El-Tantawy, F. Yakuphanoglu, Sol. Energy Mater. Sol. Cells 124 (2014) 180–185.
[18] S. Kazim, V. Alia, M. Zulfequar, M.M. Haq, M. Husain, Phys. B 393 (2007) 310–315.
[19] A. Rose, Concepts in Photoconductivity, Interscience, New York, 1963.
[20] R.K. Gupta, F. Yakuphanoglu, Sol. Energy 86 (2012) 1539.
[21] F. Yakuphanoglu, B.F. Senkal, Synth. Met. 159 (2009) 311.
[22] N. Camaioni, G. Casalbore-Miceli, G. Beggiato, M. Cristani, C. Summonte, Thin Solid Films 366 (2000) 211.
[23] S.K. Cheung, N.W. Cheung, Appl. Phys. Lett. 85 (1) (1986) .
[24] R.K. Gupta, K. Ghosh, P.K. Kahol, Phys. E 41 (2009) 617–620.
[25] S.K. Sharma, D. Pavithra, G. Sivakumar, N. Srinivasamurthy, B.L. Agrawal, Sol. Energy Mater. Sol. Cells 26 (1992) 169.
[26] B. Gunduz, A.A. Al-Ghamdi, A.A. Hendi, Z.H. Gafer, S. El-Gazzar, F. El-Tantawy, F. Yakuphanoglu, Superlattices Microstruct. 64 (2013) 167–177.
[27] G. Friesen, H.A. Ossenbrink, Sol. Energy Mater. Sol. Cells 48 (1997) 77–83.
[28] M. Saremi, M. Saremi, H. Niazi, A.Y. Goharrizi, Superlattices Microstruct. 60 (2013) 67–72.
[29] A.N. Donald, Semiconductor physics and devices, in: C.W. Wilmsen (Ed.), Physics and Chemistry of III–V Compound Semiconductor Interface, Plenum, NewYork, 1985, pp. 1992.
[30] I. Dokme, S. Altindal, T. Tunc, I. Uslu, Microelectron. Reliab. 50 (2010) 39–44.
[31] I. Dokme, S. Altindal, I. Uslu, J. Appl. Polym. Sci. (2012) , doi:http://dx.doi.org/10.1002/app.36327.
[32] E.H. Nicollian, A. Goetzberger, Bell Syst. Technol. J. 46 (1967) 1055–1133.
[33] S. Karatas, A. Turut, Vacuum 74 (2004) 45.
[34] A. Tombak, Y.S. Ocak, S. Asubay, T. Kilicoglu, F. Ozkahraman, Mater. Sci. Semicond. Process. 24 (2014) 187–192.